Proc. Natl. Acad. Sci. USA
Vol. 89, pp. 11229–11233, December 1992
Physiology

High density of Ca^{2+}-dependent K^+ and Cl^- channels on the luminal membrane of lacrimal acinar cells

(exocrine glands/electrolyte secretion/acetylcholine/ion channels)

Y. P. TAN*, A. MARTY†, AND A. TRAUTMANN†

*Boğaziçi Universitesi, BMME PK2, Bebek, Istanbul, Turkey; and †Laboratoire de Neurobiologie, Ecole Normale Supérieure, 46 rue d'Ulm, 75005 Paris, France

Communicated by Erwin Neher, August 12, 1992 (received for review March 23, 1992)

ABSTRACT **Tight-seal whole-cell recording and Ca^{2+} imaging were simultaneously performed on cell clusters or individual acinar cells of rat lacrimal glands during application of the secretagogue acetylcholine. Activation of Ca^{2+}-dependent K^+ and Cl^- currents was selectively followed as a function of time by placing the cell potential near the equilibrium potential for Cl^- or for K^+ ion, respectively. Upon acetylcholine application to cell clusters, K^+- and Cl^--selective currents displayed a distinctive initial rise ("hump"). At this time, there was only a small elevation of Ca^{2+} concentration, $[Ca^{2+}]_i$, that was restricted to the luminal end of acinar cells. A quantitative analysis of Ca^{2+} and current signals during the hump suggested that the luminal membrane contained high densities of K^+- and Cl^--selective channels, roughly 10 times higher than those found in the basolateral domain. Distinct luminal and basolateral membrane domains were preserved in isolated cells, but with less contrasted densities than in cell clusters. The results suggest that Ca^{2+}-dependent K^+ channels are implicated not only in the transfer of salt from the blood compartment to the interior of acinar cells, as commonly accepted, but also in the electrolyte secretion from the cell interior to the acinar lumen.**

Acinar cells of exocrine glands transfer ions from the blood to the acinar lumen by a Ca^{2+}-dependent process. Three types of Ca^{2+}-dependent channels, the Na,K pump, and a Na/K/Cl cotransport system have been proposed to contribute to this transfer (1–3). Cell-attached patch-clamp recordings from partially dissociated cell aggregates indicate that basolateral membranes of salivary and lacrimal glands contain all three kinds of Ca^{2+}-dependent channels, respectively selective for K^+, for Cl^-, and for monovalent cations (1–7). Very little information has been obtained on the nature of ion channels in the luminal membrane. Because of this lack of information, and of the remaining uncertainty concerning the exact composition of the fluid secreted in the acinar lumen, no agreement has been reached concerning the mechanism of secretion (1–3, 7, 8).

Kasai and Augustine (9) recently reported Ca^{2+} imaging results indicating that the Ca^{2+} rise induced by an application of the secretagogue acetylcholine (AcCho) is not spatially homogeneous. In these experiments, partially dissociated clusters of acinar cells were used. Cells in such clusters retain a marked polarity: secretory granules are exclusively found near the "luminal" region of cell-to-cell contact, whereas the nuclei are located far from the contact area, in the "basolateral" part of the cells (9). Upon AcCho application, the Ca^{2+} signal starts in the luminal part of the cells and then spreads to the basolateral side. Kasai and Augustine also compared imaging results to whole-cell recordings and have inferred that basolateral and luminal domains contain different sets of ion channels: Cl^-- and cation-selective channels on the basolateral membrane and Cl^--selective channels on the luminal membrane in their particular preparation, the exocrine pancreas. In the present work we have followed a similar, but more direct, approach by simultaneously performing Ca^{2+} imaging and patch-clamp measurements on rat lacrimal cells. Lacrimal acinar cells, like salivary acinar cells, possess a type of K^+-selective channel (BK channels) that is absent in the murine exocrine pancreas (6). It is often assumed that this channel is exclusively located in the basolateral membrane of secreting cells (1, 8). However, it has been suggested by our laboratory that BK channels may also contribute to electrolyte secretion across the luminal membrane (2, 7). The present results indicate that these channels are indeed present with high density in the luminal membrane of lacrimal cells, thus constraining secretion models for this class of exocrine glands.

METHODS

Cell Preparation. Rats (5–6 weeks old male) were anesthetized with pentobarbitone. Exorbital lacrimal glands were removed, decapsulated, and minced. Individual acinar exocrine cells and small clusters of acinar cells were obtained by successive treatments with trypsin, EGTA, and collagenase (10). Cells were then placed in modified culture dishes with a glass coverslip bottom filled with culture medium (minimum essential medium). The cells were kept in an incubator until use for 1–6 hr after dissociation.

Patch-Clamp Recording. For patch-clamp recording, cells were placed in an external saline containing (in mM) 140 NaCl, 5 KCl, 1 $CaCl_2$, 1 $MgCl_2$, and 5 NaHepes (pH 7.2). All recordings were performed at room temperature. For cell-attached and whole-cell recording, pipettes were filled with a solution containing (in mM) 140 KCl, 2 $MgCl_2$, 0.5 KEGTA, and 10 KHepes (pH 7.2). Pipettes were made from soft (hematocrit) glass. Pipette input resistance ranged from 1.5 to 3 MΩ before making the seal and from 3 to 10 MΩ in whole-cell recording.

To study the whole-cell current of the cell aggregates, we took advantage of the fact that acinar cells are linked together by gap junctions. The junctional conductance was examined using capacitive current responses to hyperpolarizing voltage steps. Only well-coupled clusters, with a gap conductance over 50 nS, were used in the present work. In well-coupled clusters, the initiation of Ca^{2+} responses in adjacent cells was consistently synchronous. In addition, ion equilibration was then relatively rapid throughout the cluster.

From previous work on this preparation, it is known that AcCho induces the activation of K^+- and Cl^--selective, Ca^{2+}-dependent channels (2). Each of the two responses can be examined in separation by choosing a membrane potential close to the Nernst potential of the other. In this study E_{Cl} and E_K were nominally at 0 and −85 mV, respectively. Since in

The publication costs of this article were defrayed in part by page charge payment. This article must therefore be hereby marked "*advertisement*" in accordance with 18 U.S.C. §1734 solely to indicate this fact.

Abbreviation: AcCho, acetylcholine.

most experiments the capacitive current of the cluster had a single exponential component, the limiting barrier for ion equilibration was at the pipette tip. The time constant for equilibration for Cl^- ions was calculated according to ref. 11 to be 70 s for the recording conditions exemplified in Fig. 1. This implies that E_{Cl} was indeed at 0 mV at the time of recording (about 7 min following break-in in this example), so that there was no significant contamination of the current at 0 mV by a Cl^--selective component. Control experiments using Cl^-/Mops or K^+/Na^+ substitution in the pipette solution suggested that small ions had equilibrated by 2 min of whole-cell recording in clusters and that errors linked to incomplete ion equilibration were negligible. A potential complication of the approach taken here is that AcCho uncouples acinar cells (12, 13). However, the time course of this phenomenon is slow, so that uncoupling need not be considered for the short stimulation times (<10 s) used in the present experiments.

AcCho Application. Applications of AcCho [0.2 or 0.25 μM, a submaximal dose (14)] were performed using a U-shaped glass capillary system (15). The onset of AcCho application triggered a light-emitting diode placed on the eyepiece of the microscope. The visual signal of the diode was used to synchronize cell current and Ca^{2+} images during off-line analysis.

Ca^{2+} Imaging. The cells were visualized with a 40× oil-immersion objective (numerical aperture, 1.3). The Ca^{2+} concentration, $[Ca^{2+}]_i$, was obtained by using fura-2 and its

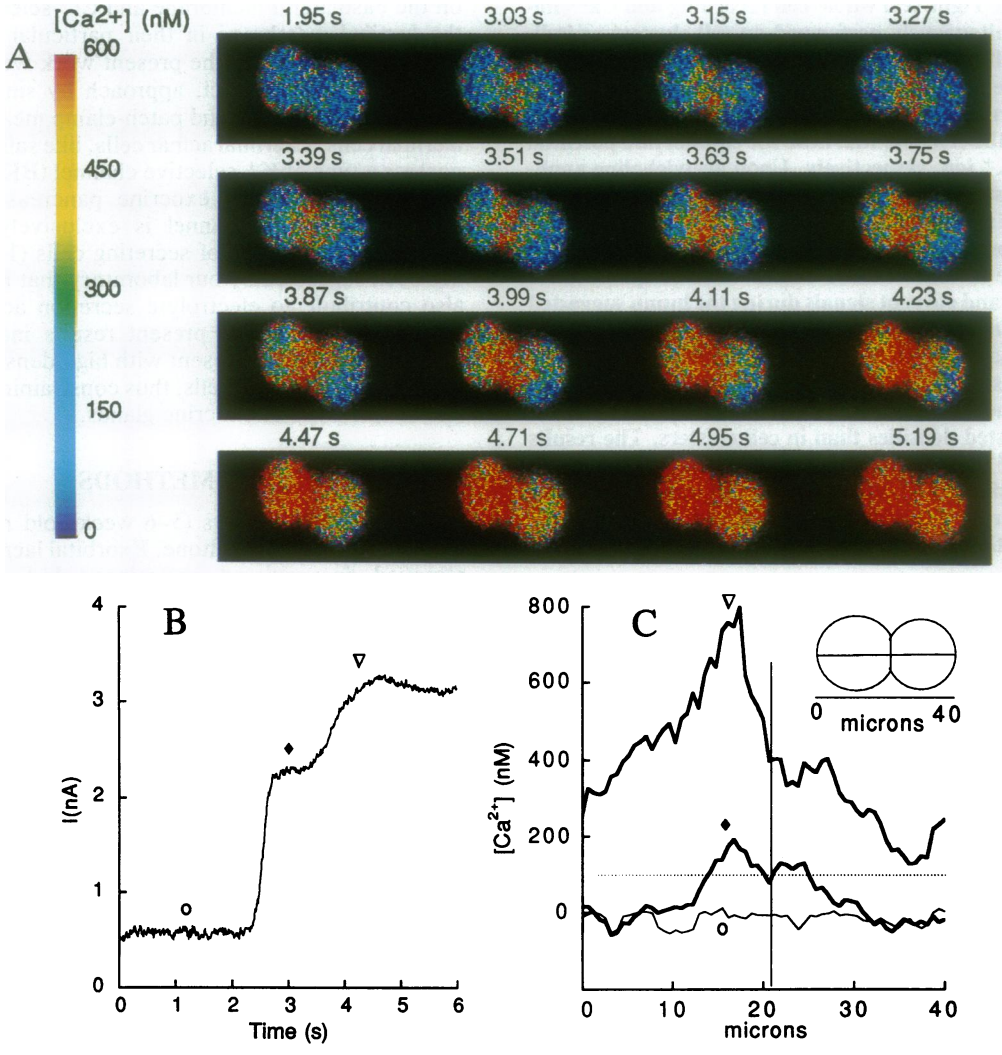

FIG. 1. Ca^{2+} imaging and Ca^{2+}-dependent K^+ current during AcCho application. (*A*) $[Ca^{2+}]_i$ images from a cell pair following local application of 0.25 μM AcCho. Time is counted from the start of AcCho application, as indicated above each image. The first image shown is representative of the low Ca^{2+} values found up to 2.8 s after AcCho application and is indistinguishable from control images taken before AcCho application. The 2nd to 12th images are 120 ms apart, and the last 5 images are 240 ms apart. (*B*) Recording of Ca^{2+}-dependent K^+ current, simultaneous to the Ca^{2+} images in *A*. The cell pair was subjected to whole-cell recording. No current change was observed until 2.3 s after the start of AcCho application. Between 2.3 and 2.8 s, the current rose abruptly to a stable level just above 2 nA (hump) and then rose again to a maximum above 3 nA. The capacitive current had a single fast component indicating an input capacitance of 31 pF. This is close to the capacitance (33 pF) calculated for the sum of two spheres of 23 μm in diameter (the mean diameter of the two cells) on the basis of a specific capacitance of 1 $\mu F/cm^2$, indicating a high degree of cell coupling by gap junctions. (*C*) $[Ca^{2+}]_i$ profiles near 1 s (○), 3.1 s (◆), and 4.3 s (▽) after the onset of AcCho application. A control Ca^{2+} profile was subtracted to only show AcCho-induced Ca^{2+} changes. Before 2.8 s, Ca^{2+} difference profiles only showed random fluctuations around 0, with peak deviations of 50 nM or less (○). During the hump a small luminal Ca^{2+} rise was observed (◆). The Ca^{2+} signal rose 100 nM or more above background over a region 10 μm wide comprising the line of cell-to-cell contact (vertical line at 21 μm). This 100 nM threshold (dotted line) corresponds to the $[Ca^{2+}]_i$ rise expected to fully activate BK channels. The Ca^{2+} difference profile was stable during the duration of the hump (between 2.8 and 3.2 s), thus allowing averaging over three consecutive images. The third profile (▽, 4.3 s) corresponds to the maximum current response. Note that the two cells still show a pronounced luminal–basolateral gradient and that the cell on the left has an average Ca^{2+} level larger than the cell on the right. Profiles at still later times showed a homogeneous high Ca^{2+} level (not shown).

lipid soluble variant fura-2 AM (16). Fura-2 was found not to diffuse readily through gap junctions, so that fura-2 AM loading was necessary (0.5 μM for 30 min in the incubator, followed by a 10-min wash at room temperature). In many experiments the pentapotassium salt of fura-2 (0.1–0.5 mM) was included in the pipette solution. In some experiments the pipette did not contain any additional fura-2. In the latter case, the useful time span for recording was limited to a few minutes after break-in due to diffusion of the dye into the pipette. In the former case, recordings were performed during the first 10 min after break-in. The Ca^{2+} images were acquired using an intensified charge-coupled device camera with a sensitivity of 10^{-5} lux (Lhesa, France). The imaging system was developed in our laboratory in collaboration with the IMSTAR Co. (Paris). This system is described in detail elsewhere (17). A reference image was acquired at 360 nm and the filter was changed to 380 nm a few seconds before AcCho application. Up to 100 images were gathered at 380 nm, and the Ca^{2+} images were computed off line using the 360-nm reference. The interval between successive images was 120 ms.

To calibrate Ca^{2+} signals, fluorescence data were obtained in individual acinar cells using various CaEGTA and Ca-HEDTA [*N*-(2-hydroxyethyl)ethylenediaminetriacetic acid, calcium salt] buffers in the pipette solution, together with fura-2. The results were fitted using the equation (16):

$$[Ca^{2+}] = K_i \frac{R - R_{min}}{R_{max} - R},$$

where R is the ratio between the 360- and 380-nm fluorescence values, R_{min} and R_{max} are the minimum and maximum of this ratio (with respective numerical values of 0.93 and 8.5), and K_i is a proportionality constant. Comparison of the fluorescence intensities in the calibration experiments with those in fura-2 AM loading indicated that the effective fura-2 concentration used in the present work was on the order of 100 μM.

Data Analysis. The first step was to subtract the background signal measured outside the cells. Then the first four to eight images were averaged during the early period of the recording (before AcCho application). This control image was subtracted from subsequent images; the resulting images are called control-subtracted images hereafter. The subtraction procedure allowed removal of the fluorescence signal due to fura-2 in the recording pipette.

Average Ca^{2+} values, or numbers of pixels where $[Ca^{2+}]_i$ exceeded a certain threshold, were determined for selected areas of the control-subtracted images. Ca^{2+} profiles were also determined on control-subtracted images. For this purpose, a line was drawn on the image. For each pixel overlapping with the line, a local Ca^{2+} average was performed over a 5 × 5 pixel area, and the resulting values were displayed as a function of distance.

All results are expressed in terms of mean ± standard deviation, and the significance of differences between two series of results is assessed using Student's *t* test.

RESULTS

Early Luminal Ca^{2+} Rise Corresponds to "Hump" of Current Response. Fig. 1 illustrates simultaneous current and Ca^{2+} responses to a local application of AcCho. After a latency of a few seconds, the Ca^{2+} signal starts in the luminal region and spreads later to the basolateral region (Fig. 1). In this experiment, the potential was set at 0 mV, so that K^+-selective currents were recorded. In agreement with previous findings (10, 15), there was a distinctive early component (hump) of the K^+-selective current observed in response to AcCho (Fig. 1*B*). This hump was simultaneous with the very beginning of the luminal Ca^{2+} response (Fig. 1*C*), suggesting that the luminal current density was larger than that of the basolateral area.

To analyze the spatio-temporal relation between $[Ca^{2+}]_i$ and Ca^{2+}-dependent currents, Ca^{2+} levels were averaged within small areas of the luminal and basolateral regions, and the resulting luminal and basolateral Ca^{2+} signals were compared with the K^+ and Cl^- currents. Fig. 2 *A* and *B* depict the result of the first kind of experiment. The luminal response is coincident with the hump, whereas the basolateral response corresponds to the second, delayed current rise. Similar results were obtained with the Cl^--selective current (Fig. 2 *C* and *D*).

Current–Pixel Plots. Let us consider the K^+ response and assume that it is entirely due to BK channels (2, 18, 19). At 0 mV, BK channels are partially activated at resting $[Ca^{2+}]_i$ and are further activated following AcCho-induced Ca^{2+} rise (18). BK channels have a steep Ca^{2+} dependence corresponding to a 6-fold increase in the opening probability, p_o, for a doubling of $[Ca^{2+}]_i$ (20). Therefore even modest local $[Ca^{2+}]_i$ changes are likely to activate fully the channels. The data can thus be interpreted in terms of a Ca^{2+} wave activating BK channels in an all-or-none manner. As an estimate of the area of active membrane the number of pixels that had a $[Ca^{2+}]_i$ value above a certain threshold were counted. This number was related to the current recorded at the same time. The resulting plot (Fig. 3*A*) displays two linear parts corresponding to the activation of the luminal and basolateral domains, respectively. The transition between the two linear parts corresponds to the hump in the current trace. In practice, the threshold for the pixel count was chosen near twice the resting $[Ca^{2+}]_i$—i.e., 100–200 nM above this concentration. The features of pixel–current plots depended little on the threshold value (from 50 to 250 nM above rest). In the example shown, the first and second

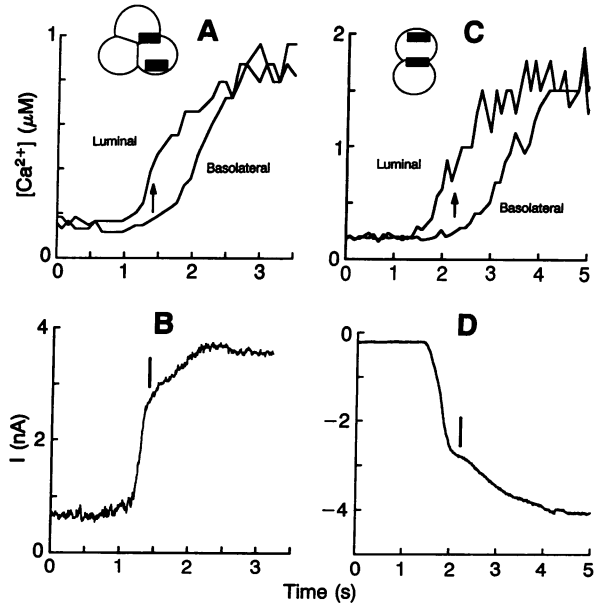

FIG. 2. Ca^{2+} signal in the luminal membrane domain is synchronous with the hump of Ca^{2+}-dependent current. (*A*) Recordings of average $[Ca^{2+}]_i$ calculated on small luminal and basolateral domains of an aggregate of three cells. (*B*) Corresponding K^+ current response recorded at 0 mV. (*C*) Recordings of average $[Ca^{2+}]_i$ calculated in luminal and basolateral domains (shaded areas) from a cell pair. (*D*) Simultaneous recording of Cl^- current response at −85 mV. Short vertical marks (*B* and *D*) and arrows (*A* and *C*) are indicated to facilitate visual comparison between the timing of the luminal signal and the hump of the Ca^{2+}-dependent currents. Zero time corresponds to the onset of AcCho application.

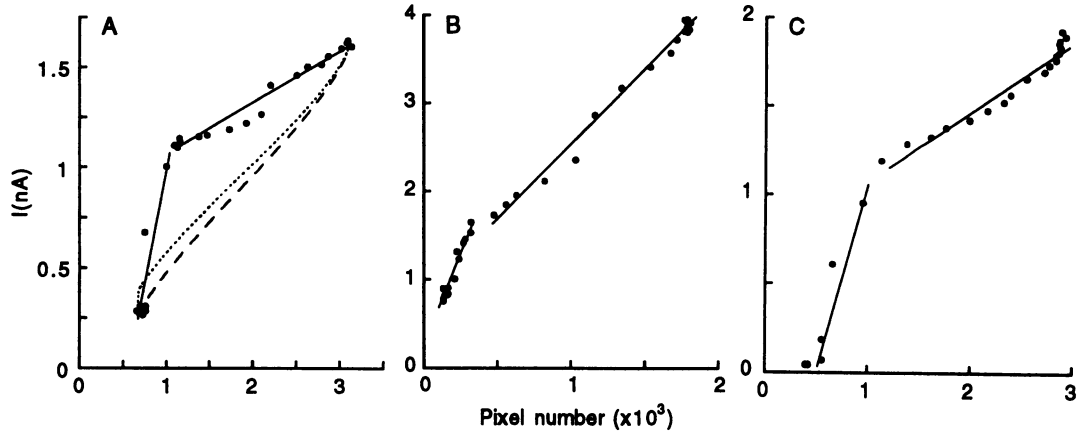

FIG. 3. Current–pixel plots yield two linear regions. All three plots were generated using control-subtracted Ca^{2+} images. A threshold increment of 200 nM Ca^{2+} was chosen for all plots. The number of pixels exceeding this threshold was determined for each Ca^{2+} image, over the whole cell cluster. This number was plotted as a function of the amplitude of the corresponding current during AcCho application. Least square linear fits to each region are shown. (*A*) Cell pair. K^+ current recorded at 0 mV. The slopes of the linear fits are 2.23 pA per pixel (luminal) and 0.26 pA per pixel (basolateral). (*B*) Single cell. K^+ current recorded at 0 mV. Slopes of linear fits are 2.2 pA per pixel and 0.85 pA per pixel. (*C*) Cell pair. Cl^- current recorded at −85 mV. Slopes of linear fits are 2.0 pA per pixel and 0.39 pA per pixel. The dotted and dashed lines in *A* indicate the predictions of models where channels are supposed to be homogeneously distributed on the membrane of the cells, approximated by two spheres flattened at the region of contact. Relevant distances were measured on the bright field image. The models assume that a Ca^{2+} wave having planar boundaries parallel to the central contact region progresses symmetrically, activating Ca^{2+}-dependent channels in an all-or-none manner. Two variants are presented, depending on whether channels are distributed only on the spherical surface (dashes) or whether the surface of contact is also included (dots).

slope values were 2.23 and 0.26 pA per pixel, respectively. Corresponding average values were 1.75 ± 0.86 and 0.10 ± 0.07 pA per pixel (Table 1). These results indicate a considerable difference of current density between luminal and basolateral domains, with a mean slope ratio of 13.0 ± 8.0. If the cells were flattened disks (an assumption that will be examined below), then the membrane surface area would amount to twice the pixel area for each pixel—i.e., $2 \times 0.36 = 0.72\ \mu m^2$. Taking a single channel current of 7 pA at 0 mV for BK channels (4) and a maximum p_o close to 1 (20), the calculated channel densities are 0.42 per μm^2 in the luminal domain and 0.03 per μm^2 in the basolateral domain.

Assuming that the number of pixels above threshold and the area of active membrane are proportional, the ratio of luminal to basolateral areas equals the ratio of pixel ranges for the steep and shallow parts of the current–pixel plots. This ratio was 0.06 in the example of Fig. 3*A* and averaged 0.09 ± 0.03 ($n = 7$) for the cell clusters analyzed at 0 mV, where humps were apparent.

To assess the validity of the above analysis, we calculated the outcome of current–pixel plots for a homogeneous current distribution over two adjacent flattened spheres. In one plot (dashes in Fig. 3*A*), currents were supposed to be nil over the planar contact area, whereas currents were assumed to be equally distributed over the entire surface in the other plot (dots in Fig. 3*A*). Both curves are in sharp contrast to the experimental data (Fig. 3*A*), confirming that the channel density is not homogeneous in cell pairs. Note that the dashed line is not far from a straight line. This shows that the above approximation of a cell pair by two disks was acceptable.

Current–pixel plots were also performed on AcCho-induced responses obtained in individual cells. Such cells are known to retain some polarization, with secretory vesicles clustering at a luminal end of the cell and the nucleus marking the opposite basolateral end (21). Using peroxidase labeling to stain secretory granules, such clustering was clearly observed in about half of the isolated cells in our hands (results not shown). Upon application of AcCho, a rather large proportion of cells displayed humps in the initial current rise (Table 1; see also ref. 10). The cells with humps gave biphasic current–pixel plots (Fig. 3*B*). On average, however, the slope ratio derived from individual cells was significantly smaller ($P < 0.02$) than that obtained with cell clusters. Furthermore,

Table 1. Analysis of basolateral/luminal current densities

Recording conditions	% of cells with humps*	*I* (luminal),† %	Slope: Basolateral,‡ pA per pixel	Slope: Luminal,§ pA per pixel	Slope ratio¶	*n*‖
I_K (cell clusters)	78	46 ± 27	0.10 ± 0.07	1.75 ± 0.86	13 ± 8	9
I_K (individual cells)	57	25 ± 30	0.44 ± 0.30	2.0 ± 1.2	3.7 ± 4.0	7
I_{Cl} (cell clusters)	75	47 ± 36	0.30 ± 0.10	2.5 ± 2.1	6.0 ± 5.2	8

The number of pixels with $[Ca^{2+}]_i$ above threshold was counted for successive Ca^{2+} images during AcCho application. Current values obtained at 0 mV (for I_K measurements) or −85 mV (for I_{Cl} measurements) were averaged over short periods around the time for image acquisition. Measurements were performed either on individual cells or on cell clusters (two or three cells), as indicated. Plots of current against pixel numbers were fitted using two separate linear regressions if a clear break was apparent and with a single linear regression in the other cases.

*Proportion of cells with humps in the current trace.

†Fraction of the total current obtained at the time of the hump. When no hump was apparent, a value of 0 was entered.

‡Basolateral slopes. When no break was apparent in the current–pixel plot, the slope of the overall linear regression was entered.

§Average luminal slopes. No value was entered in the cases of uniform slope.

¶Average slope ratios. When a single slope could be determined this ratio was set at 1. Slope ratios excluding such cases were 16.5 ± 4.8 (I_K, clusters), 5.7 ± 4.4 (I_K, individual cells), and 7.9 ± 4.8 (I_{Cl}, clusters).

‖Total number of experiments for each situation.

the average basolateral slope was significantly larger ($P < 0.01$) in the former situation than in the latter. The fact that single cells often yielded a biphasic current–pixel plot suggests that such plots are not an artefact linked with the presence of a contact area between adjacent cells—a conclusion also in line with the observation that on two occasions cell clusters displayed an initial luminal Ca^{2+} signal and yet gave essentially linear current–pixel plots. On the other hand, the results on slope ratio and on basolateral slopes indicate that a significant redistribution of luminal channels over the entire membrane occurs for individual cells.

Current–pixel plots were finally made of responses obtained at −85 mV, yielding results similar to those obtained at 0 mV (Fig. 3*C*; Table 1).

Cell-Attached Recordings. As an alternative to the present interpretation of the results, it could be proposed that the initiation of the Ca^{2+} response takes place not only in the luminal part of the cells but also in a very thin basolateral domain just beneath the plasma membrane (22). In such a case, the first phase of the response could contain a large contribution from basolateral channels, even though the corresponding Ca^{2+} rise would remain undetected. To test this possibility, cell-attached experiments were performed on basolateral locations together with Ca^{2+} imaging. It was found that basolateral K^+ channels were not activated during the luminal Ca^{2+} response. Only during the basolateral phase of the Ca^{2+} response did a clear and sudden increase of p_o occur (three recordings). These results confirm that the basolateral membrane takes no part in the generation of the early current response.

DISCUSSION

The main result of the present work is that the initiation of the Ca^{2+} response in lacrimal glands is accompanied by the activation of a high density of K^+- and Cl^--selective currents in the luminal membrane of acinar cells. According to the current–pixel analysis summarized in Table 1, current densities are 13 times and 6 times larger in the luminal membrane (K^+ and Cl^- currents, respectively) than in the basolateral membrane. These figures must be taken with some caution, given the numerous simplifications involved in the analysis. It is unclear whether the region of contact should be classified as luminal and whether or not it contributes to the recorded currents. The simulation of Fig. 3*A* suggests, however, that the relative contribution of this area to the total cluster surface is too small to affect the conclusions seriously. It is possible that the current densities are even more contrasted than suggested by the current–pixel analysis. This is because intrinsic Ca^{2+} gradients may be spread out by the very presence of fura-2 (23) and by the spatial filtering introduced by the limited resolution of the optics, so that the site of origin of the luminal response may be more restricted in space than the results indicate.

It remains to be seen whether luminal and basolateral channels have exactly the same properties. Assuming similar or identical channel types, the high current densities found in the luminal membrane translate into high densities of channel numbers. Electron microscopy results indicate that the surface area of the luminal domain is much smaller than that of the basolateral membrane (21). Likewise, our current–pixel plots indicate that the luminal membrane accounts only for 9% of the total surface area. Thus, the high density of luminal channels ensures that ion fluxes through the basolateral and luminal membrane are matched during steady-state secretion. The fact that well-defined membrane domains exist in the present preparation indicates that the severe disruption of tight junctions, which undoubtedly accompanies the formation of small aggregates, does not lead to a random redistribution of luminal and basolateral channels over the entire cell membrane. Thus other mechanisms, such as anchoring to cytoskeleton elements, must be responsible for keeping the basolateral/luminal segregation (24).

The results are difficult to reconcile with secretion models that place Ca^{2+}-dependent K^+ channels exclusively on the basolateral membrane (1, 8). On the other hand, they are fully compatible with an alternative model that assumes the presence of Ca^{2+}-dependent K^+ and Cl^- channels on the basolateral membrane and on the luminal membrane (2, 7).

Y.P.T. gratefully acknowledges the support of Centre National de la Recherche Scientifique and the North Atlantic Treaty Organization during completion of this work. This work was also supported by grants from the Centre National de la Recherche Scientifique (URA 295) and from the Université Pierre et Marie Curie.

1. Petersen, O. H. & Maruyama, Y. (1984) *Nature (London)* **307**, 693–696.
2. Marty, A., Tan, Y. P. & Trautmann, A. (1984) *J. Physiol. (London)* **357**, 293–325.
3. Petersen, O. H. (1992) *J. Physiol. (London)* **448**, 1–51.
4. Marty, A., Evans, M. G., Tan, Y. P. & Trautmann, A. (1986) *J. Exp. Biol.* **124**, 15–32.
5. Maruyama, Y. & Petersen, O. H. (1982) *Nature (London)* **299**, 159–161.
6. Randriamampita, C., Chanson, M. & Trautmann, A. (1988) *Pflügers Arch.* **411**, 53–57.
7. Marty, A. (1987) *Trends Neurosci.* **10**, 373–377.
8. Suzuki, K. & Petersen, O. H. (1985) *Q. J. Exp. Physiol.* **70**, 437–445.
9. Kasai, H. & Augustine, G. J. (1990) *Nature (London)* **348**, 735–738.
10. Marty, A. & Tan, Y. P. (1989) *J. Physiol. (London)* **419**, 665–687.
11. Pusch, M. & Neher, E. (1988) *Pflügers Arch.* **411**, 204–211.
12. Iwatsuki, N. & Petersen, O. H. (1978) *J. Physiol. (London)* **274**, 81–96.
13. Neyton, J. & Trautmann, A. (1986) *J. Physiol. (London)* **377**, 283–295.
14. Horn, R. & Marty, A. (1988) *J. Gen. Physiol.* **92**, 145–159.
15. Krishtal, O. A. & Pidoplichko, V. I. (1980) *Neuroscience* **5**, 2325–2327.
16. Grynkiewicz, G., Poenie, M. & Tsien, R. Y. (1984) *J. Biol. Chem.* **260**, 3440–3450.
17. Donnadieu, E., Cefai, D., Tan, Y. P., Paresys, G., Bismuth, G. & Trautmann, A. (1992) *J. Immunol.* **148**, 2643–2653.
18. Trautmann, A. & Marty, A. (1984) *Proc. Natl. Acad. Sci. USA* **81**, 611–615.
19. Findlay, I. (1984) *J. Physiol. (London)* **350**, 179–195.
20. Barrett, J. N., Magleby, K. L. & Pallotta, B. S. (1982) *J. Physiol. (London)* **331**, 211–230.
21. Herzog, V., Sies, H. & Miller, F. (1976) *J. Cell Biol.* **70**, 692–706.
22. Foskett, J. K., Gunter-Smith, P. J., Melvin, J. E. & Turner, R. J. (1989) *Proc. Natl. Acad. Sci. USA* **86**, 167–171.
23. Neher, E. & Augustine, G. J. (1992) *J. Physiol. (London)* **450**, 273–301.
24. Carraway, K. L. & Carothers Carraway, C. A. (1989) *Biochim. Biophys. Acta* **988**, 147–171.